Revisiting the LuGre Friction Model

KARL JOHAN ÅSTRÖM and
CARLOS CANUDAS-DE-WIT

STICK-SLIP MOTION AND RATE DEPENDENCE

Friction is a classical field that dates back to Leonardo da Vinci, Guilliame Amonton, and Charles Augustin de Coulomb [1]–[3]. Amonton found that friction force is proportional to normal load but surprisingly is independent of the area of the apparent contact surface. This observation is known as the Amonton's paradox. The *apparent* contact surface is the geometric object surface projected to the contact surface. The *true* contact surface is the actual surface in contact between the object and the surface. The apparent contact surface is typically much larger than the effective contact surface. However, measurements of the contact surface of rocks [4] show that the friction force is proportional to true contact area, finally resolving Amonton's paradox.

Coulomb proposed a model where the friction force is opposite to the direction of velocity with a magnitude proportional to the normal force. Major advances in understanding the mechanisms generating friction were made by Bowden and Tabor [5] and by the tribologist Rabinowizc [6], who performed extensive experiments to understand the macroscopic properties of friction. By measuring the velocity dependence of friction in ball bearings, Stribeck [7] found that friction decreases with increasing velocity in certain velocity regimes. This phenomenon is called the Stribeck effect. Friction models developed in the physics community also include the *rate-and-state models*, in which friction is a function of the velocity and a state variable, [8]–[10].

Major advances in understanding friction have recently become possible because of the availability of measurement techniques and equipment such as scanning probe microscopy, laser interferometry, and the surface force apparatus, which make it possible to measure friction at the nanoscale [11], [12].

Friction also plays a major role in control systems. It limits the precision of positioning and pointing systems and can give rise to instabilities [13]–[16]. The effects of friction can be alleviated to some extent by friction compensation [17]–[20]. For control applications, it is useful to have

Digital Object Identifier 10.1109/MCS.2008.929425

1066-033X/08/$25.00©2008IEEE

simple models that capture the essential properties of friction. Two examples are the linear viscous friction model and the Coulomb friction model. These memoryless models have limitations because they cannot reproduce phenomena such as stick-slip motion.

Indeed, friction is known to have dynamic behavior [21], [22]. Phenomena such as predisplacement, rate dependence, and hysteresis have been observed experimentally and are reproduced only by dynamic models. The Dahl model [23], [24], developed in the late 1960s, is a simple dynamic model with one state and is widely used to simulate aerospace systems [23], [25]. Several friction models are used in civil engineering [26] to describe how concrete structures respond when subjected to strong seismic excitations. The main motivation is to characterize the behavior of a structure that is excited beyond its elastic range.

The Dahl model does not capture the Stribeck effect and thus cannot predict stick-slip motion. The LuGre model [20], [27]–[29], named to recognize that it originated in a collaboration between the control groups in Lund and Grenoble, is an extension of the Dahl model that captures the Stribeck effect and thus can describe stick-slip motion. The LuGre model contains only a few parameters and thus can easily be matched to experimental data. This model has passivity properties [30] that are useful for designing friction compensators that give asymptotically stable closed-loop systems [28], [31]. The LuGre model has been applied to a wide range of systems [31]–[34]. Although experiments generally show good agreement with the LuGre model, discrepancies are observed in [31]. To overcome these discrepancies several modifications are considered in [35]–[37] based on the Preisach, Duhem, Maxwell-slip, and Bouc-Wen models. In addition, ad hoc extensions of the LuGre model based on the inclusion of a deadzone to separate the plastic and elastic zones are considered in [22].

In this article we first review properties of the LuGre model, including zero-slip displacement, invariance, and passivity. An extension to include velocity-dependent microdamping is also discussed. The resulting model is then used to analyze stick-slip motion. The analysis shows that stick-slip motion modeled by the LuGre model is a stiff system with different behavior in the stick and slip modes as well as dramatic transitions between these modes. The dependence of limit cycles on parameters is discussed along with the notion of rate dependence.

The Dahl Model

The starting point for modeling friction in mechanical servos is an observation made by Dahl [23] in 1968, namely, that ball-bearing friction is similar to solid friction. This similarity is illustrated by the experimental data shown in Figure S1. The figure shows that the amplitude decays linearly rather than exponentially. The linear decay of the amplitude is compatible with Coulomb friction. Dahl found a similar behavior when he replaced the pendulum with a mass on a piano wire. The observation inspired Dahl to base a friction model on the stress-strain curve. A simple version is the exponential function

$$F = F_c(1 - e^{-\sigma_0|x|/F_c})\operatorname{sgn}\left(\frac{dx}{dt}\right), \tag{S1}$$

where F is the force (proportional to stress), x is the displacement (proportional to strain), σ_0 is the stiffness, and F_c is the Coulomb friction force. Differentiating (S1) yields

$$\begin{aligned}\frac{dF}{dx} &= \sigma_0\left(1 - \frac{F}{F_c}\operatorname{sgn}\left(\frac{dx}{dt}\right)\right)\\ &= \sigma_0\left(1 - \frac{F}{F_c}\operatorname{sgn}(v)\right).\end{aligned} \tag{S2}$$

Introducing $z = F/\sigma_0$ as a state variable, and using the chain rule we find

$$\frac{dz}{dt} = \frac{1}{\sigma_0}\frac{dF}{dx}\frac{dx}{dt} = \frac{1}{\sigma_0}\frac{dF}{dx}v = v - \frac{\sigma_0}{F_c}|v|z, \tag{S3}$$

which is the Dahl friction model. In steady state we have $z = z_0 = F_c\operatorname{sgn}(v)/\sigma_0$. This result implies that

$$F_{ss} = \sigma_0 z_0 = F_c\operatorname{sgn}(v). \tag{S4}$$

The friction model (S3) is a first-order dynamic system whose steady-state behavior gives Coulomb friction (S4). The state z represents the displacement $z = F/\sigma_0$ corresponding to the friction force F. The state can also be interpreted as the local strain or the average bristle deflection as described in [46]. The model has two parameters, namely, σ_0, and F_c. The model captures many properties of friction in mechanical systems [29], and has been used extensively to simulate friction, particularly for precision pointing systems. However, the Dahl model does not capture the Stribeck effect and the associated stick-slip motion.

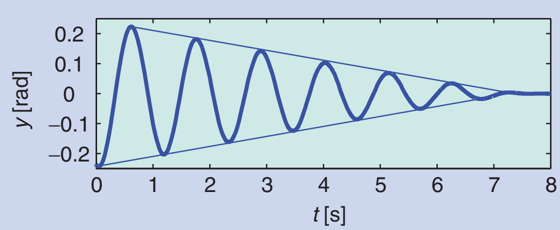

FIGURE S1 Oscillation of a pendulum supported by ball bearings. Notice that the amplitude decays linearly, indicating that ball-bearing friction is similar to solid friction.

THE LUGRE MODEL

The LuGre model is described by

$$\dot{z} = v - \sigma_0 \frac{|v|}{g(v)} z = v - h(v)z, \tag{1}$$

$$F = \sigma_0 z + \sigma_1 \dot{z} + f(v), \tag{2}$$

where v is the velocity between the two surfaces in contact, z is the internal friction state, and F is the friction force. Compared with the Dahl model described in "The Dahl Model," the LuGre model has a velocity-dependent function $g(v)$ instead of a constant, an additional damping σ_1 associated with microdisplacement, and a general form $f(v)$ for the memoryless velocity-dependent term. The state z, which is analogous to the strain in the Dahl model, can be interpreted as the average bristle deflection. The LuGre model reproduces spring-like behavior for small displacements, where the parameter σ_0 is the stiffness, σ_1 is the microdamping, and $f(v)$ represents macrodamping, typically viscous friction $f(v) = \sigma_2 v$. For constant velocity, the steady-state friction force F_{ss} is given by

$$F_{ss}(v) = g(v)\,\mathrm{sgn}(v) + f(v), \tag{3}$$

where $g(v)$ captures Coulomb friction and the Stribeck effect. A reasonable choice of $g(v)$ giving a good approximation of the Stribeck effect is

$$g(v) = F_c + (F_s - F_c)e^{-|v/v_s|^{\alpha}}, \tag{4}$$

where F_s corresponds to the stiction force, and F_c is the Coulomb friction force. A typical shape of $g(v)$ is shown in Figure 1, where $g(v)$ takes values in the range $F_c \le g(v) \le F_s$. The parameter v_s determines how quickly $g(v)$ approaches F_c. The value $\alpha = 1$ is suggested in [13], while [38] finds values in the range 0.5–1, and [21] uses $\alpha = 2$.

The functions $f(v)$ and $g(v)$ in (3) can be determined experimentally by measuring steady-state friction force for various constant velocities. Such a measurement gives the function $F_{ss}(v)$ in (3). To have a complete model we must also determine the parameters σ_0, σ_1. In practice we find that friction in motors may be asymmetric. This asymmetry can be handled by using different values of the parameters for positive and negative values of the velocity. For simplicity of exposition, however we assume symmetry.

Boundedness and Dissipativity

We now consider properties of the LuGre model (1), (2), with $g(v)$ as in (4) and $f(v) = \sigma_2 v$.

Property 1 [Boundedness]

It follows from (4) that $0 < g(v) \le F_s$. Then, $\Omega = \{z : |z| \le F_s/\sigma_0\}$ is an invariant set for the LuGre model. That is, if $|z(0)| \le F_s/\sigma_0$, then $|z(t)| \le F_s/\sigma_0$ for all $t \ge 0$.

Property 1 is a consequence of the fact that the time derivative of the quadratic function $V = z^2/2$ along solutions of (1) is given by

$$\dot{V} = z\left(v - \sigma_0 \frac{|v|}{g(v)} z\right) = -|v||z|\left(\sigma_0 \frac{|z|}{g(v)} - \mathrm{sgn}(v)\mathrm{sgn}(z)\right).$$

Note that $\sigma_0(|z|/g(v)) \ge 0$ and that $\mathrm{sgn}(v)\,\mathrm{sgn}(z)$ takes the values 1 or -1. When $\mathrm{sgn}(v)\,\mathrm{sgn}(z) = -1$, it follows that $(\sigma_0(|z|/g(v)) - \mathrm{sgn}(v)\,\mathrm{sgn}(z))$ is positive, and hence $\dot{V}$ is negative semidefinite. Alternatively, when $\mathrm{sgn}(v)\,\mathrm{sgn}(z) = 1$ and $|z| > g(v)/\sigma_0$, it follows that $\dot{V}$ is negative. Since $g(v)$ is positive and bounded by F_s, we see that the set Ω is an invariant set for the solutions of (1). For further details, see [28].

Property 1 indicates that if the internal state z is initially below the upper bound of the function $g(v)$, that is, below the normalized stiction force F_s/σ_0, then the state remains bounded, specifically, $z(t) \le F_s/\sigma_0$ for all $t \ge 0$.

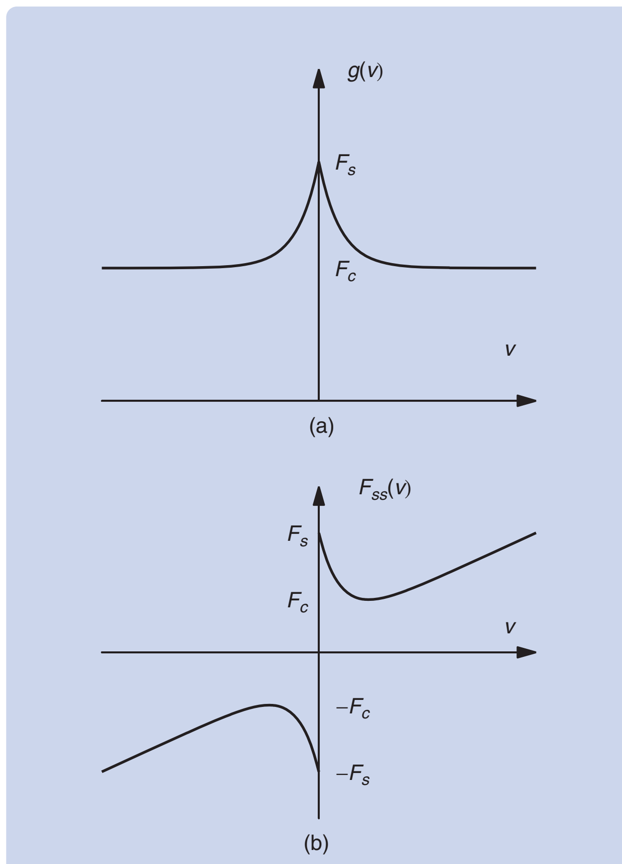

FIGURE 1 Functions that characterize the LuGre friction model. (a) shows the function $g(v)$ that captures Coulomb friction and the Stribeck effect, while (b) shows the steady-state friction function $F_{ss}(v) = g(v)sgn(v) + f(v)$, where $f(v)$ represents viscous friction, typically, $f(v) = \sigma_2 v$. F_c is the Coulomb friction force, whereas F_s denotes the stiction force. Asymmetric friction behavior can be obtained by letting $g(v)$ and $F(v)$ have different shapes for positive and negative velocities.

Passivity is related to energy dissipation. The following results summarize the passivity properties of the LuGre model.

Property 2 [Internal State Dissipativity]

The map $v \mapsto z$ defined by (1) is dissipative with respect to the storage function $W(z(t)) = (1/2)z^2(t)$, that is,

$$\int_0^t z(\tau)v(\tau)\, d\tau \geq W(z(t)) - W(z(0)), \quad \text{for all } t \geq 0. \tag{5}$$

Property 2 indicates that the LuGre model is input-to-state passive [39] for all positive values of the model parameters. Next, we wish characterize conditions under which the input-to-output (I/O) map $v \mapsto F$ is also passive, that is, there exists $\beta > 0$ such that $\int_0^t Fv \geq -\beta$ for all $t \geq 0$. For details, see [28] and [40].

Property 3: [I/O Dissipativity with Constant σ_1]

The map $v \mapsto F$, defined by (1) and (2) has the property

$$\begin{aligned}\int_0^t Fv\, d\tau &\geq W(z(t)) - W(z(0)) + \rho \int_0^t v^2 d\tau \\ &\geq -W(z(0)), \quad \text{for all } t \geq 0,\end{aligned} \tag{6}$$

which implies that the map is input strictly passive with $\rho = \sigma_2 - \sigma_1(F_s - F_c/F_c) > 0$ and with the storage function $W(z) = (\sigma_0/2)z^2$ if and only if

$$\sigma_2 > \sigma_1 \frac{(F_s - F_c)}{F_c}. \tag{7}$$

The sufficiency of Property 3 is shown in [29], while the necessity is proven in [30]. The passivity condition (7) requires that the viscous damping coefficient σ_2 be sufficiently large. This condition is a minor constraint when F_s and F_c are close, but may be quite restrictive when F_s is significantly larger than F_c. The effect of σ_1 is discussed further in the next sections.

Velocity-Dependent Microdamping

The parameter σ_1 represents the damping in the predisplacement regime. The influence of σ_1 outside this regime is negligible since $\dot{z}$ tends to zero on a faster time scale than $v(t)$ when the system leaves the predisplacement zone where the velocity v is close to zero.

The impact of σ_1 on the ability of the model to accurately predict friction forces depends on the particular application. For systems where slow motions in the micro- and nanoscales are crucial (atomic force microscopes, satellite antennas, ultrasonic motors), σ_1 is a critical parameter that must be determined by using sensors with high resolution and bandwidth. However, in mechanical systems where the sensor resolution and its expected accuracy are within the millimeter scale (industrial robots, tool machines, drives), the effect of σ_1 is minor, and its main role is to damp the linearized equation in the presliding regime rather than to finely match the data in a region where the sensed information (position and velocity) is rather poor. In the latter case, imposing a given damping ratio ζ in the presliding regime gives $\sigma_1 = 2\zeta\sqrt{\sigma_0 m} - \sigma_2$, with the typical choice of $\zeta = 1$, to obtain well-behaved stick-slip transitions.

The passivity condition (7) yields the condition

$$\zeta < \frac{\sigma_2}{2\sqrt{\sigma_0 J}} \left(\frac{F_c}{F_s - F_c} + 1 \right) \tag{8}$$

on the damping ratio of the micromotion. In some applications, obtaining both passivity and critical damping may be difficult. This difficulty can be overcome by using a velocity-dependent function $\bar{\sigma}_1(v)$, where these two properties can be set independently.

Property 4 [I/O Dissipativity with Velocity-Dependent $\bar{\sigma}_1(v)$]

Suppose that $\bar{\sigma}_1(v)$ satisfies the following conditions:

i) $|v|\bar{\sigma}_1(v) < 4g(v), \quad \text{for all} \quad v,$

ii) $\bar{\sigma}_1(0) = \sigma_1 \triangleq 2\zeta\sqrt{\sigma_0 m} - \sigma_2.$

Then, the map $v \mapsto F$ defines an input strictly passive operator, $\int_0^t Fv\, d\tau \geq W(z(t)) - W(z(0)) + \sigma_2 \int_0^t v^2 d\tau$, for all $T \geq 0$, with the storage function $W(z) = (\sigma_0/2)z^2$.

If the function $\bar{\sigma}_1(v) > 0$ decays exponentially, then the function $|v|\bar{\sigma}_1(v)$ is positive and concave. Since $F_c \leq g(v) \leq F_s$, for all v, condition i) is satisfied if $\max_v\{|v|\bar{\sigma}_1(v)\} < 4F_c$. The function $\bar{\sigma}_1(v) = \sigma_1 e^{-(v/v_c)^2}$ with $\sigma_1 \triangleq 2\zeta\sqrt{\sigma_0 m} - \sigma_2$ and $v_c < 4\sqrt{2e}\,F_c/\sigma_1$ satisfies conditions i) and ii). By choosing a velocity-dependent microdamping $\bar{\sigma}(v)$, it is thus possible to obtain a model that is passive and has good microdamping. The transition rate from stick to slip is governed by the parameter v_c. This parameter can be chosen sufficiently small to satisfy $\bar{\sigma}_1(v) = \sigma_1 e^{-(v/v_c)^2}$ and make $\bar{\sigma}_1(v)$ vary fast enough so that the rate of variation of the product $\bar{\sigma}_1(v)\dot{z}$ is dominated by the rate of variation of $\bar{\sigma}_1(v)$. In that way, $\bar{\sigma}_1(v)\dot{z} \approx \sigma_1\dot{z}$ when $v \approx 0$, and $\bar{\sigma}_1(v)\dot{z} \approx 0$ when $v > \epsilon$. The local behavior of the system in stiction is well damped, while the dissipation I/O property of the model is recovered. Note that this behavior holds for arbitrarily large parameters.

Micromotion or Zero-Slip Displacement

Micromotion, which is also called the zero-slip behavior, can be explored in an experiment where an external force F_d that is smaller than the stiction force is applied to a mass at rest. Using the LuGre model, the experiment can be modeled by

$$\dot{x} = v, \tag{9}$$

$$m\dot{v} = F_d - F, \tag{10}$$

$$\dot{z} = v - \sigma_0 \frac{|v|}{g(v)} z, \tag{11}$$

$$F = \sigma_0 z + \sigma_1 \dot{z}, \tag{12}$$

where x is the displacement and the viscous damping is neglected for simplicity. Equations (9)–(12) have an equilibrium $v = 0$ and $z = z_0 = F_d/\sigma_0$ if $|F_d| < F_s$. Linearizing around this equilibrium yields

$$m\ddot{z} + \frac{F_s - F_d}{F_s}\sigma_1\dot{z} + \frac{F_s - F_d}{F_s}\sigma_0 z = 0. \tag{13}$$

The motion of the friction state z is thus characterized by second-order, spring-mass-damper dynamics. For $F_d = 0$ the undamped natural frequency is $\omega_0 = \sqrt{m/\sigma_0}$ and the damping ratio is $\zeta = 0.5\sigma_1/\sqrt{m\sigma_0}$. The system is critically damped when $\sigma_1 = 2\sqrt{m\sigma_0}$. The frequency and the damping decreases with increasing F_d and the system (13) becomes unstable for $F_d = F_s$.

If the time profile of the external force F_d has zero dc component and its magnitude is small compared to the stiction force F_s, then the friction behaves as a pure spring force, that is, $F \approx \sigma_0 x$, as described by the linearized equation (13). In this case the elastic effect dominates the plastic effect, and hence the model exhibits a *return-to-zero* position when the external force is set back to zero. Nevertheless, if the applied force F_d has a constant bias, then the system exhibits zero-slip displacement, as shown in the next experiment.

A simulation of the experiment is shown in Figure 2. The force is applied at time $t = 0$, set to zero at $t = 0.02$, and reapplied at $t = 0.04$. When the force is applied, the system reacts like a spring, the mass moves a small distance, and the friction force builds up as the friction state z is increased. The system settles at steady state with a small displacement. When the force is set to zero, the state returns to zero, but the mass does not return to its original position. This phenomenon is called zero-slip displacement [21].

The friction forces predicted by the Dahl and LuGre models cover the elastoplastic domain. The accumulated drift on the mass position is due to small excursions from the purely elastic region, where the models are approximately linear. This effect, called *position drift* in stiction or *plastic sliding*, is also exhibited by other models as discussed in detail in [41].

STICK-SLIP MOTION

Stick-slip motion is a common behavior associated with friction. Everyday examples are the squeaking sounds when opening a door, braking a car, or writing on a blackboard with a chalk. A typical stick-slip experiment is

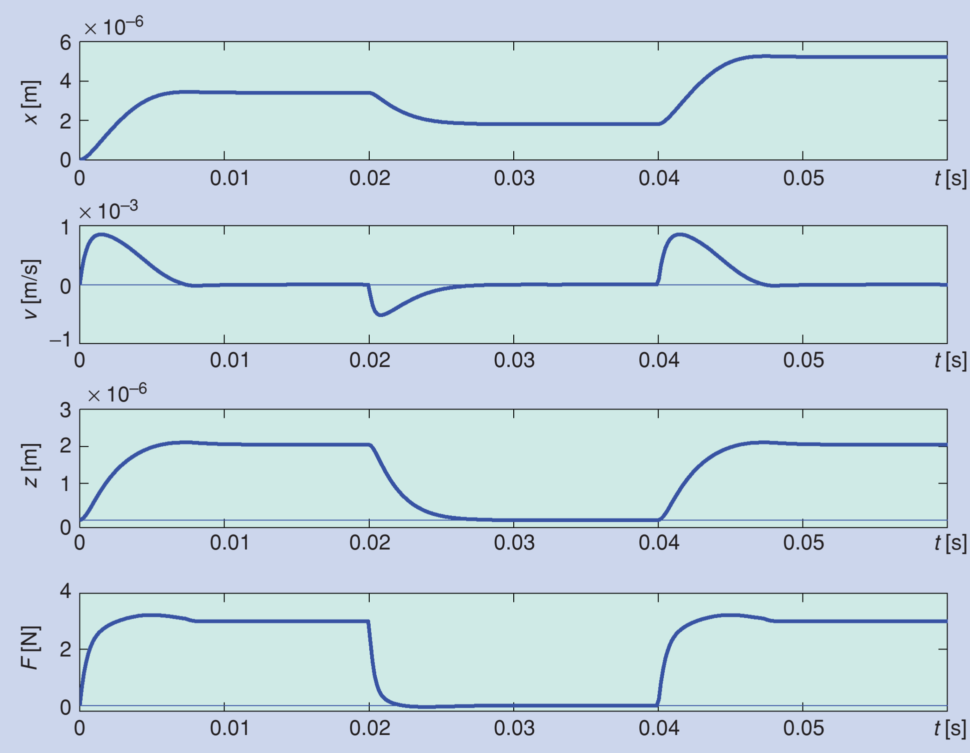

FIGURE 2 Simulation of start-stop experiment. The force $F < F_s$ is applied to a mass at time $t = 0$. The force is set to zero at time $t = 0.1$ and is applied again at time $t = 0.2$. When the force is applied, the system initially reacts like a spring, the mass moves a small distance, and the friction force builds up as the friction state z increases. The system settles at steady state with a small displacement. When the force is set back to zero, the state returns to zero, but the mass does not return to its original position. The net motion obtained, which is called *zero-slip displacement*, can be attributed to the nonlinear nature of the model, which introduces small excursions from the purely elastic regions where the model is approximately linear. Parameters used in the simulation are $m = 1$ kg, $\alpha = 1$, $\sigma_0 = 1.47 \times 10^6$ N/m, $\sigma_1 = 2.42 \times 10^3$ kg/s, $\sigma_2 = 0$ kg/s, $F_c = 2.94$ N, $F_s = 5.88$ N, and $v_s = 0.001$ m/s.

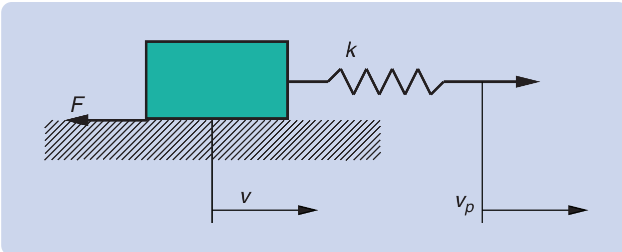

FIGURE 3 Stick-slip experiment. The mass is attached to a spring k, which is pulled at constant speed. In response, the mass alternates between sticking and slipping.

to pull string connected to a mass as shown in Figure 3. The mass, which is initially at rest, is pulled at a constant rate. When the spring is elongated so that the force exerted by the spring exceeds the stiction force, the mass accelerates. The spring is then compressed, and, under certain conditions, the motion of the mass stops and the process repeats, creating a periodic motion consisting of phases where the mass sticks and slips. A simple hybrid model gives some insight into the limit-cycle behavior; see "A Hybrid Model for Stick-Slip Motion."

A Hybrid Model for Stick-Slip Motion

A simple model of stick-slip motion is obtained by considering two modes, namely stick and slip. In the stick mode the mass is stationary, and the spring is pulled with velocity v_p. Let ℓ be the elongation of the spring. In the stick mode the elongation of the spring is given by

$$\frac{d\ell}{dt} = v_p. \tag{S5}$$

The system remains in the stick mode as long as the spring force is smaller than the stiction force F_s. Letting k be the spring coefficient, we find that the mass is stuck as long as velocity is zero and $|\ell| < \ell_s$, where $\ell_s = F_s/k$ is the elongation of the spring required to give the stiction force F_s. In the sliding mode the mass moves subject to the spring force, and the friction force is modeled as Coulomb friction $F = -F_c \operatorname{sgn}(v)$. The equation of motion in the slipping mode is

$$\frac{d\ell}{dt} = v_p - v, \tag{S6}$$

$$m\frac{dv}{dt} = k\ell - F_c \operatorname{sgn} v = k(\ell - \ell_c \operatorname{sgn} v), \tag{S7}$$

where $\ell_c = F_c/k$. The system remains in the slip mode as long as $v \neq 0$ or $v = 0$, and $|\ell| > \ell_s$.

The system is a hybrid system with two states, *stick* and *slip*. The system is in the *slip* state when $v \neq 0$ or $v = 0$ and $|\ell| > \ell_s$ and in the *stick* state otherwise.

Simulation of the hybrid model requires care. Integration routines with event detection are required to avoid missing switches, which can yield misleading results since the mass may not stick [46]. In our particular case the equations can be integrated analytically. In the stick mode we have $v = 0$, and $\ell = v_p t + c_1$ where c_1 is a constant. Integrating the equations for the slip mode yields

$$m(v - v_p)^2 + k(\ell - \ell_c)^2 = c_2, \tag{S8}$$

where c_2 is a constant. With proper scaling the trajectories are circles or circle segments in the ℓ, v plane with centers at $\ell = \ell_c$ and $v = v_p > 0$. The circle segment corresponds to the slip mode, whereas the line segment corresponds to the stick mode. Patching the solutions we find that the system is described by the phase plane shown in Figure S2.

The stick mode is the line segment $v = 0$ and $|\ell| < \ell_s$; see Figure S2. The trajectories are segments of circles with centers at $(\ell_c,\ v_p\sqrt{m/k})$ for positive v. If the trajectory hits the stick mode, it moves toward the right. At the right end of the stick mode the solution follows the circle segment counterclockwise until it hits the stick mode. Trajectories starting outside the dashed circle converge to the limit cycle. Convergence is fast; the solution is on the limit cycle as soon as it reaches the stick mode and moves past the point $v = 0$ and $l = 2\ell_c - \ell_s$. Trajectories inside the dashed line are circles. The center, corresponding to the mass moving at the pulling rate, is also stable but not asymptotically stable.

It is easy to see what happens when parameters of the model are changed. For viscous friction the circle segments are replaced by logarithmic spirals, and the center becomes stable. The limit cycle disappears when the damping is large.

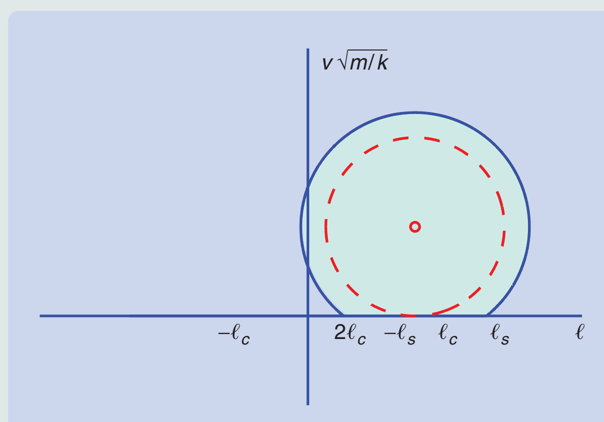

FIGURE S2 Phase plane for the hybrid model of stick-slip motion. The sticking mode is the line $v = 0$ and $2\ell_c - \ell_s \le \ell \le \ell_s$. The slipping motion forms arcs of circles with centers at $(\ell_c,\ v_p\sqrt{m/k})$ for $v + p > 0$. The center is marked with a circle. The dashed curve is a circle with center at $(\ell_c, v_p\sqrt{m/k})$ and radius $v_p\sqrt{m/k}$, which just touches the slip mode. All trajectories starting outside this circle converge to the limit cycle.

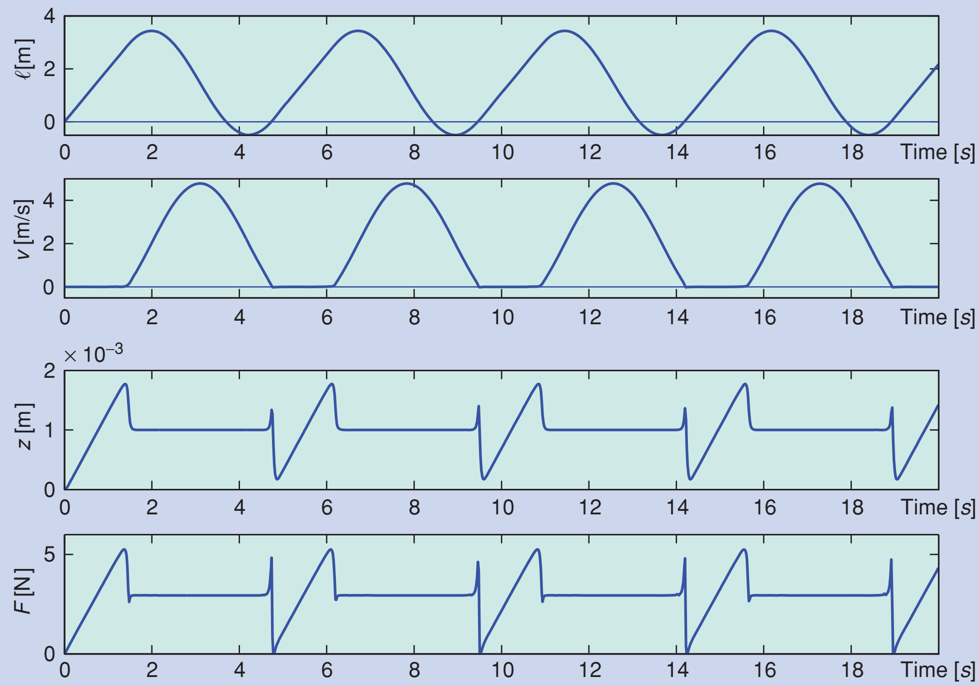

FIGURE 4 Behavior of the system in Figure 3 when the right-hand side of the spring is pulled with constant velocity. The graphs show the elongation ℓ of the spring, velocity v of the mass, the state z of the friction model, and the friction force F. The parameters are $m = 1$ kg, $k = 2$ N/M, and $v_p = 2$ m/s. The function g is given by (4) with parameters $\alpha = 1$, $\sigma_0 = 2940$ N/M, $\sigma_1 = 108$ kg/s, $\sigma_2 = 0$ kg/s, $F_c = 2.94$ N, $F_s = 5.88$ N, and $v_s = 0.001$ m/s.

Stick-Slip Behavior of the LuGre Model

We now analyze the stick-slip experiment using the LuGre friction model. Introducing the elongation ℓ of the pulling spring, the experiment can be described by

$$\dot{\ell} = v_p - v, \tag{14}$$

$$m\dot{v} = k\ell - F, \tag{15}$$

$$\dot{z} = v - \sigma_0 \frac{|v|}{g(v)} z = v - z\,h(v), \tag{16}$$

where $h(v) \triangleq \sigma_0 |v|/g(v)$, and the friction force F is given by

$$F = \sigma_0 z + \sigma_1 \dot{z} + f(v) = \sigma_1 v + f(v) + (\sigma_0 - \sigma_1 h(v))z. \tag{17}$$

The simulation in Figure 4 shows that a stable limit cycle with stick-slip motion is rapidly established. Stick regimes appear, for example, between 4.8 s and 6.2 s, where the velocity is very small and is repeated periodically. When the trajectory enters the stick mode the friction state increases rapidly, and the friction force effectively stops the motion. Friction state z and friction force F then drop rapidly before increasing almost linearly to compensate for the force from the spring. When the spring force is larger than the stiction force, the mass starts to move, and the friction force drops rapidly with a small overshoot. Notice that the friction state and the friction force have similar shapes.

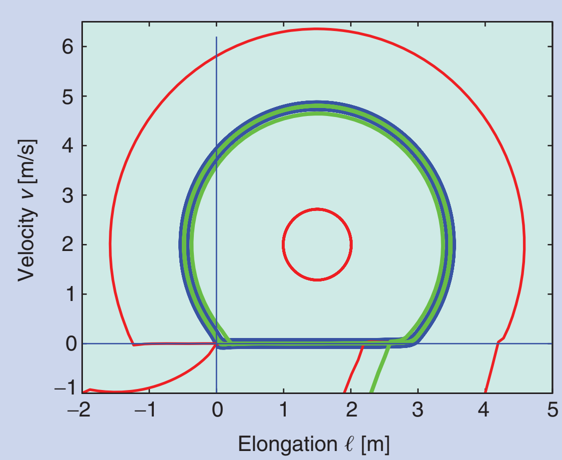

FIGURE 5 Projections of trajectories of the third-order system (14)–(16) on the $v - \ell$ plane. The stick-slip motion is the heavy blue line. All trajectories starting outside the blue line approach stick-slip motion. Trajectories starting close to the equilibrium give sinusoidal nonsliding motion, whereas trajectories starting inside but close to the limit cycle converge to stick-slip motion.

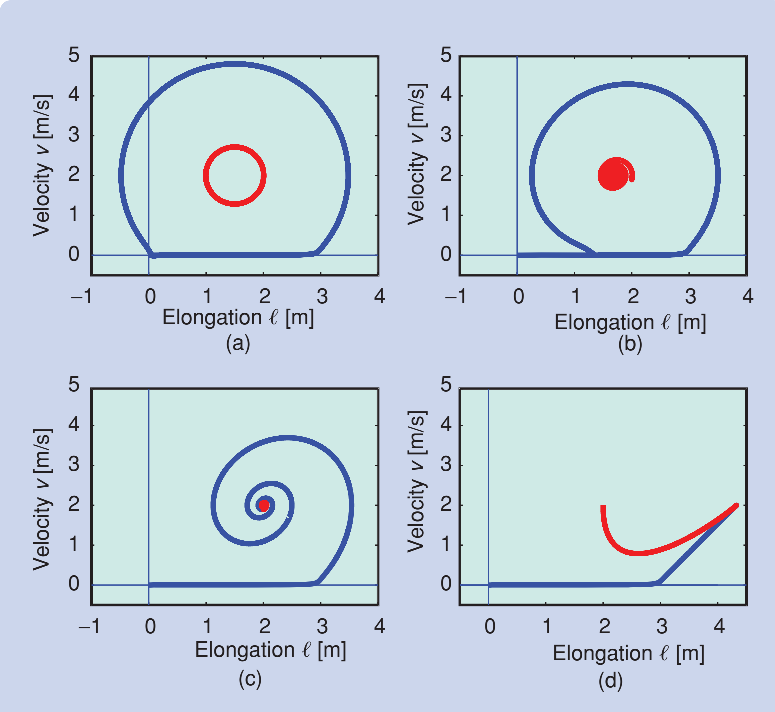

FIGURE 6 Change of behavior with viscous friction σ_2. The equilibrium shifts to the right with increasing values of σ_2; see (23)–(25). The equilibrium in (a) is Lyapunov stable but not asymptotically stable. The equilibrium becomes asymptotically stable for $\sigma_2 > 0$, and shifts to the right with increasing σ_2. The equilibrium is critically damped for $\sigma_2 = 2\sqrt{2}$ kg/s in (d). The limit cycle shrinks when σ_2 changes from 0 to 0.2 in (b), and it disappears for larger values of σ_2, as shown in (c) and (d). The parameter values are (a) $\sigma_2 = 0$, (b) $\sigma_2 = 0.2$ kg/s, (c) $\sigma_2 = 0.5$ kg/s, and (d) $\sigma_2 = 2\sqrt{2}$ kg/s.

The gross features of the behavior of the LuGre model are similar to those obtained with the hybrid model, but the transitions are now captured by dynamics instead of logic. The hybrid model is a second-order system, while the LuGre model is a third-order system. To compare the models, the solution of the LuGre model is projected on the $\ell - v$ plane as shown in Figure 5. Comparing Figure 5 and Figure S2 shows that the limit cycles have similar shapes. Trajectories starting outside the limit cycles, or inside and close to it, converge to the limit cycle representing stick-slip motion. Trajectories starting close to the equilibrium do not entail stick slip. There are also some subtle differences. The projections of the red and green trajectories of the LuGre model in Figure 5, starting at $v = -1$ with ℓ close to 2, cross each other, but the corresponding trajectories for the hybrid model cannot cross because the system is of second order.

Considerable insight can be obtained by making some approximations. In Figure 4 we can recognize two distinct modes, the stick mode, where the velocity is close to zero, and the slip mode, where the friction state z is constant. There are also transitions between the modes. Let us first investigate the slip phase where the state z is essentially constant. Assuming that $\dot{z}$ is small, (17) reduces to the second-order system

$$\dot{\ell} = v_p - v, \tag{18}$$

$$\begin{aligned} m\dot{v} &= k\ell - f(v) - \sigma_0 z \\ &= k\ell - f(v) - g(v)\mathrm{sgn}(v) \\ &= k\ell - F_{ss}(v), \end{aligned} \tag{19}$$

where F_{ss} is the steady-state friction function given by (3). Linearizing the system we find that the dynamics matrix is

$$A = \begin{bmatrix} 0 & -1 \\ k/m & F'_{ss}(v_0) \end{bmatrix}. \tag{20}$$

In the slip mode the system is thus approximately described by second-order spring-mass-damper dynamics with natural frequency $\omega_{\mathrm{slip}} = \sqrt{k/m}$ and damping given by $F'_{ss}(v) = dF_{ss}(v)/dv$. Since viscosity is zero in the simulation in Figure 4, the function F_{ss} is constant in the slip phase, which implies that damping is absent.

Next we investigate the behavior in the stick mode. Since Figure 4 shows that the velocity is small in the stick mode, we linearize (14)–(16) and obtain a linear system with the dynamics matrix

$$A = \begin{bmatrix} 0 & -1 & 0 \\ \dfrac{k}{m} & -\dfrac{\sigma_1(1 - zh'(v)) + f'(v)}{m} & -\dfrac{\sigma_0 - \sigma_1 h(v)}{m} \\ 0 & 1 - zh'(v) & -h(v) \end{bmatrix}. \tag{21}$$

Assuming that $f(v) = \sigma_2 v$ and that v and z are small yields

$$A = \begin{bmatrix} 0 & -1 & 0 \\ \dfrac{k}{m} & -\dfrac{\sigma_1 + \sigma_2}{m} & -\dfrac{\sigma_0}{m} \\ 0 & 1 & 0 \end{bmatrix}. \tag{22}$$

The characteristic polynomial of (22) is given by

$$p(s) = s\left(s^2 + \frac{\sigma_1 + \sigma_2}{m} + \frac{\sigma_0 + k}{m}\right).$$

The dynamics are characterized by an integrator and an oscillatory system with natural frequency $\omega_{\mathrm{stick}} = \sqrt{(\sigma_0 + k)/m}$.

For control applications, it is useful to have simple models that capture the essential properties of friction.

The presence of the integrator explains the linear time evolution of z and F in the stick modes (small v) of Figure 4, while the large value of ω_{stick} explains the rapid variations in the transition from stick to slip. Modeling stick slip by the LuGre model shows that the gross behavior is characterized by two modes. In the slip mode the dynamics are approximately second-order spring-mass-damper dynamics with the characteristic frequency $\omega_{\text{slip}} = \sqrt{k/m}$. We call behavior the macrodynamics. In the stick mode the dynamics are characterized by an integrator along with spring-mass-damper dynamics with the characteristic frequency $\omega_{\text{stick}} = \sqrt{(\sigma_0 + k)/m}$. Since σ_0 is much larger than k, the ratio $\omega_{\text{stick}}/\omega_{\text{slip}}$ is large, making the system stiff. A dramatic change in dynamics occurs in the transition between the modes. In the simulation in Figure 4 we use a smaller value of σ_0 in order to show the transition more clearly. The transition zone shrinks as σ_0 increases.

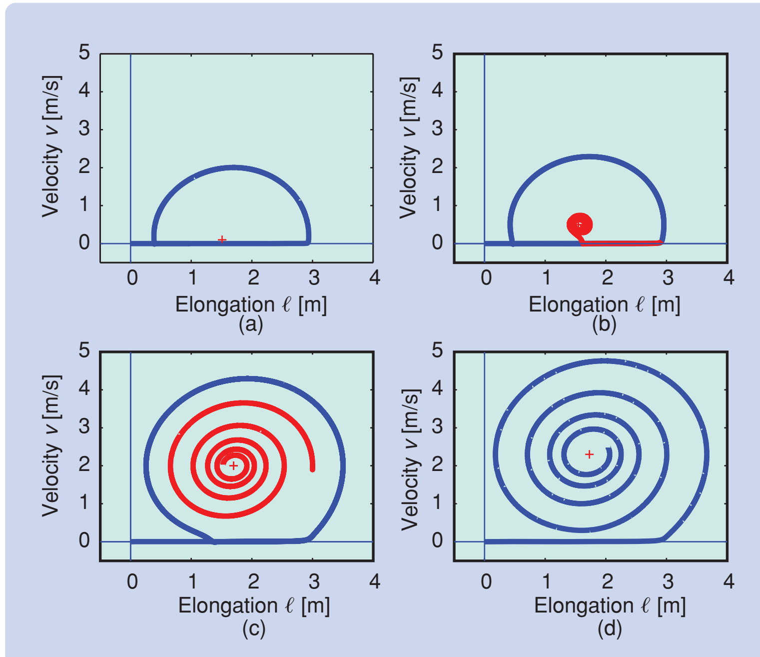

FIGURE 7 Change of behavior with pulling velocity v_p. The equilibrium shifts vertically with increasing v_p and, to a smaller degree, in the horizontal direction; see (23)–(25). The equilibrium is unstable for low v_p as shown in (a) unless the damping is very large. All solutions then approach the limit cycle. The equilibrium moves upward when the pulling velocity increases as shown in (c). The left part of the limit cycle shrinks, and the limit cycle disappears when the pulling velocity is sufficiently large, as shown in (d). The equilibrium is then also asymptotically stable, stick-slip motion disappears, and the mass moves steadily with constant velocity. The parameter values are (a) $v_p = 0.002$ m/s, (b) $v_p = 0.005$ m/s, (c) $v_p = 0.02$ m/s, and (d) $v_p = 0.023\sqrt{2}$ m/s

Effects of Parameter Changes

We now investigate the effect of parameter variations on the limit cycles. First we observe that (14)–(16) has the equilibrium

$$\ell_e = \frac{F_{ss}(v_p)}{k}, \tag{23}$$

$$v_e = v_p, \tag{24}$$

$$z_e = \frac{v_p}{h(v_p)} = \frac{g(v_p)}{\sigma_0}\,\mathrm{sgn}(v_p), \tag{25}$$

where the function $F_{ss}(v)$ is the steady-state friction function

$$F_{ss}(v) = g(v)\,\mathrm{sgn}(v) + f(v) = F_c + (F_s - F_c)e^{-|v/v_s|^{\alpha}} + \sigma_2 v. \tag{26}$$

The equilibrium (23)–(25) corresponds to the situation in which the mass is moving forward at the constant pulling velocity v_p. The stability of this equilibrium can be determined by linearizing the system (14)–(16). A straightforward calculation shows that the dynamics matrix has the characteristic polynomial

$$p(s) = s^3 + a_1 s^2 + a_2 s + a_3, \tag{27}$$

where

$$\begin{aligned} a_1 &= \frac{\sigma_1(1 - zh'(v)) + f'(v)}{m} + h(v) \\ &= \frac{\sigma_1 v g'(v) + f'(v)g(v)}{mg(v)} + \frac{\sigma_0|v|}{g(v)}, \\ a_2 &= \frac{\sigma_0(1 - zh'(v)) + f'(v)h(v) + k}{m} \\ &= \frac{\sigma_0|v|}{g(v)} F'_{ss}(v) + \frac{k}{m}, \\ a_3 &= \frac{kh(v)}{m} = \frac{\sigma_0 k|v|}{mg(v)}. \end{aligned}$$

The Routh-Hurwitz criterion implies that the equilibrium is asymptotically stable if and only if a_1, a_2, and a_3 are positive and $a_1 a_2 > a_3$.

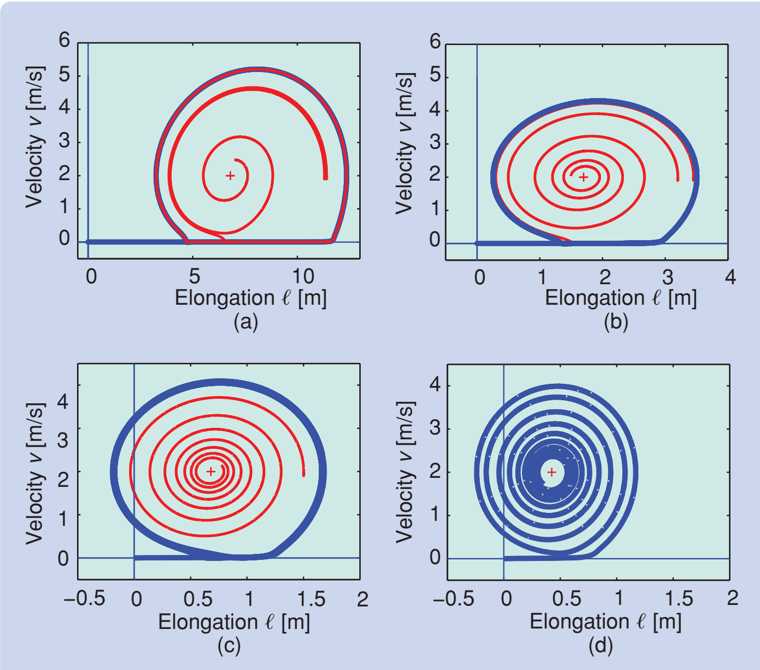

FIGURE 8 Change of behavior with spring coefficient k. The equilibrium shifts toward the left with increasing spring coefficient. For $k = 2$ N/m, (a) shows two red trajectories, one converges to the equilibrium while the other converges to the limit cycle. As k increases, the region of attraction of the equilibrium increases as shown in (b) and (c). The limit cycle disappears when k is sufficiently large as shown in (d). The stiffness is (a) $k = 0.5$ N/m, (b) $k = 2$ N/m, (c) $k = 5$ N/m, and (d) $k = 8$ N/m.

Consider the effect of viscous damping, where $f(v) = \sigma_2 v$. To discuss the resulting behavior we focus on the equilibrium given by (23)–(25) and the limit cycle corresponding to stick-slip motion. It follows from (23) and (26) that the equilibrium shifts to the right (increasing ℓ) with increasing damping. Figure 6 shows stick-slip behavior for several values of σ_2. For small values of σ_2 the equilibrium changes from being Lyapunov stable for $\sigma_2 = 0$ to asymptotically stable for $\sigma_2 > 0$. Solutions far from the equilibrium approach the limit cycle, but the limit cycle disappears for large values of σ_2. Figure 6(d) shows trajectories for $\sigma_2 = 2\sqrt{2} = 2.824$ kg/s, the equilibrium at $v_0 = 2$ m and $\ell_0 = 4.3$ m is critically damped.

Next we investigate the effect of the pulling velocity v_p. It follows from (24) that changes in v_p shift the equilibrium vertically as shown in Figure 7. Figure 7 shows stick-slip behavior for several values of v_p. For low-pulling velocities the equilibrium is close to the ℓ axis and, unless the viscous damping is very large, is unstable. The limit cycle is then asymptotically stable. As the pulling velocity increases, the equilibrium (23)–(25) changes from unstable to stable, while the limit cycle remains a locally stable solution. For large values of v_p the limit cycle disappears.

A bifurcation occurs when the equilibrium (23)–(25) changes from unstable to stable. The analytical condition for the transition is that the quantity

$$
\begin{aligned}
a_1 a_2 - a_3 &= \left(\frac{\sigma_0 |v|}{g} + \frac{\sigma_1 g' v + f' g}{mg}\right) \\
&\quad \times \left(\frac{\sigma_0 |v|}{g} F'_{ss} + \frac{k}{m}\right) - \frac{\sigma_0 k |v|}{mg} \\
&= \sigma_0^2 \frac{v^2}{g^2} F'_{ss} + \sigma_0 \frac{|v|}{mg^2} (\sigma_1 g' v + f' g) F'_{ss} \\
&\quad + \frac{k(\sigma_1 g' v + f' g)}{m^2 g} \\
&\approx \sigma_0^2 \frac{v^2}{g^2} F'_{ss} \\
&= h^2 F'_{ss}
\end{aligned}
$$

changes sign from positive to negative. The arguments v of the functions f, g, F and their derivatives have been suppressed to avoid clutter. The approximate expression is

Rate Independence of the Dahl Model

The Dahl model is one of the simplest friction models that is rate independent. Naively, rate independence follows from the fact that the model is derived from the stress-strain curve. Formally, rate independence can be shown as follows. Let $\varphi : t \mapsto \tau$ be an increasing homeomorphism, that is, $\varphi' \triangleq (\partial\varphi/\partial t) > 0$ mapping the time $t \in [0, \infty)$ to the transformed time $\tau \in [0, \infty)$, where $\tau = \varphi(t)$. To demonstrate that the hysteresis operator $H : v \mapsto F$ associated with the Dahl model (S2)

$$\frac{1}{\sigma_0}\frac{dF}{dt} = v - \frac{F}{F_c}|v| \tag{S9}$$

is rate independent, we need to show that, for every input-output pair, $(v(t), F(t))$, that satisfies (S9), the corresponding scaled pair $(v_\tau(\tau), F(\tau))$, with $v_\tau = dx/d\tau$, satisfies the time-scaled equation. Using the chain rule, and the fact that $|v_\tau \varphi'| = |v_\tau|\varphi'$, which follows from $\varphi' > 0$, we obtain

$$\varphi' \left\{\frac{1}{\sigma_0}\frac{dF}{d\tau} - v_\tau + \frac{F}{F_c}|v_\tau|\right\} = 0.$$

Again using $\varphi' > 0$ we find that $(v_\tau(\tau), F(\tau))$ is an admissible solution of

$$\frac{1}{\sigma_0}\frac{dF}{d\tau} = v_\tau - \frac{F}{F_c}|v_\tau|.$$

Stick-slip motion modeled by the LuGre model is a stiff system with different behavior in the stick and slip modes as well as dramatic transitions between these modes.

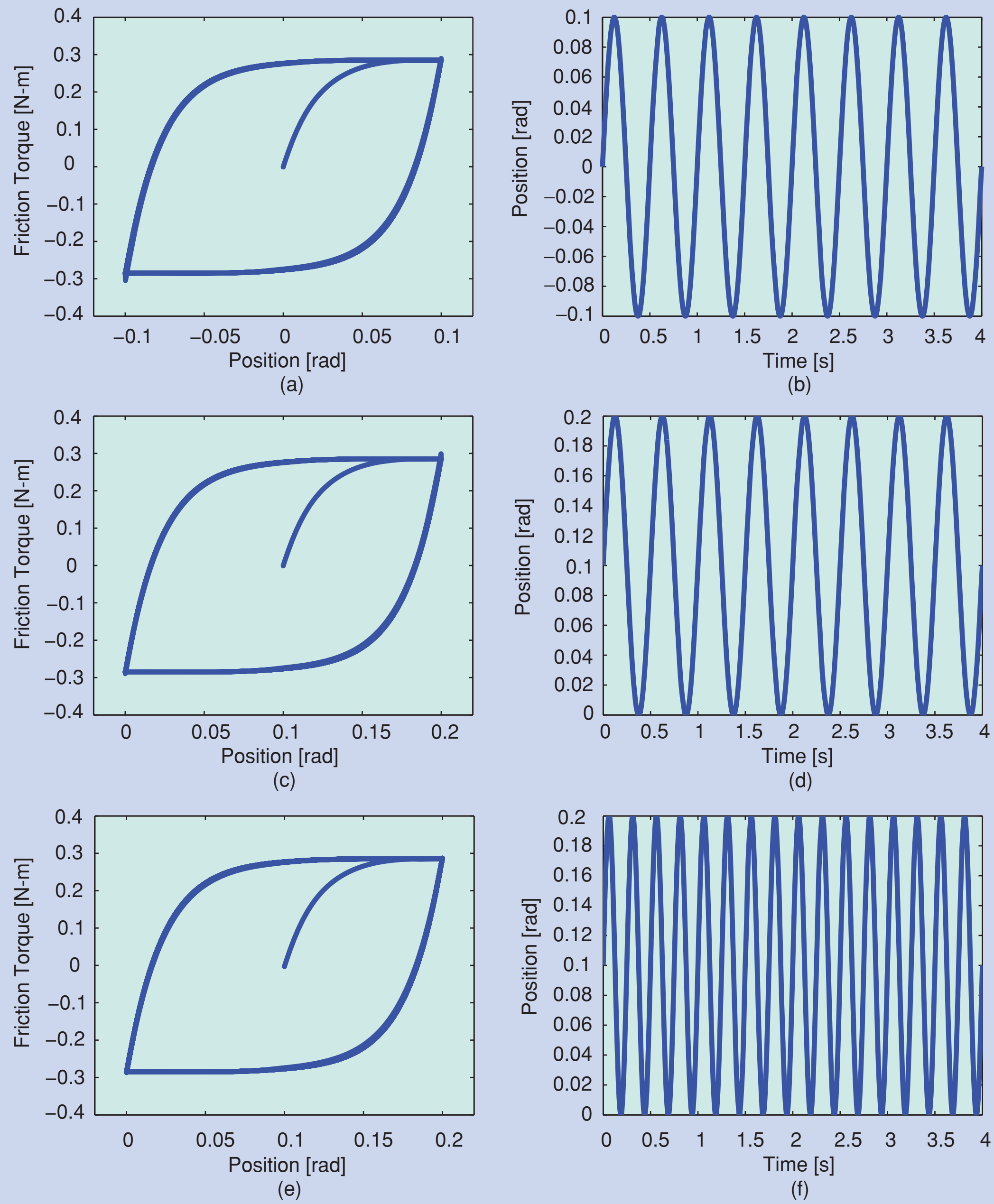

FIGURE 9 Illustration of the rate-independent property of the Dahl model. The left plots show phase planes, while the right plots show the position as a function of time. The input is sinusoidal with frequency 2 Hz in (a)–(d). A constant is added to the input in the experiment shown in (c) and (d); the output is shifted, but the shape remains the same. The plots (e)–(f) show that the limit cycle remains the same when the frequency at the input is changed to 4 Hz.

> **The LuGre model is a dynamic friction model with a few parameters that can be fitted by measuring steady-state friction as a function of velocity.**

obtained by observing that the σ_0^2-term dominates. The approximate condition implies that the equilibrium is unstable when the pulling velocity is in the range where the slope of the static friction curve is negative.

Mechanical systems where the inertia forces can be neglected and internal friction generates hysteretic behavior are examples of systems that may be rate independent. For example, in the presliding regime, where inertial forces can be neglected, every point of the velocity reversals is recovered in the force-position plane once the force resumes the corresponding value, independently of the number of velocity reversals [14]. In the literature of systems with hysteresis, this property is sometimes termed as *reversal point memory* [25]. In "Rate Independence of the Dahl Model," it is shown that the Dahl model is rate independent. The models discussed in [42]–[44] are also rate independent.

Consider a rate-independent friction model. If the input velocity $v(t)$ is periodic, then the steady-state output force $F(t)$ is also periodic, and hence closed loops are formed in the input-output (force-velocity) $F-v$ plane, as well as in the force-position $F-x$ plane. Since the system is rate invariant the loops are invariant to changes in the frequency of the input signal. By the rate-independent property, these hysteresis loops are invariant with respect to time scaling, and thus invariant with respect to the input signal frequency.

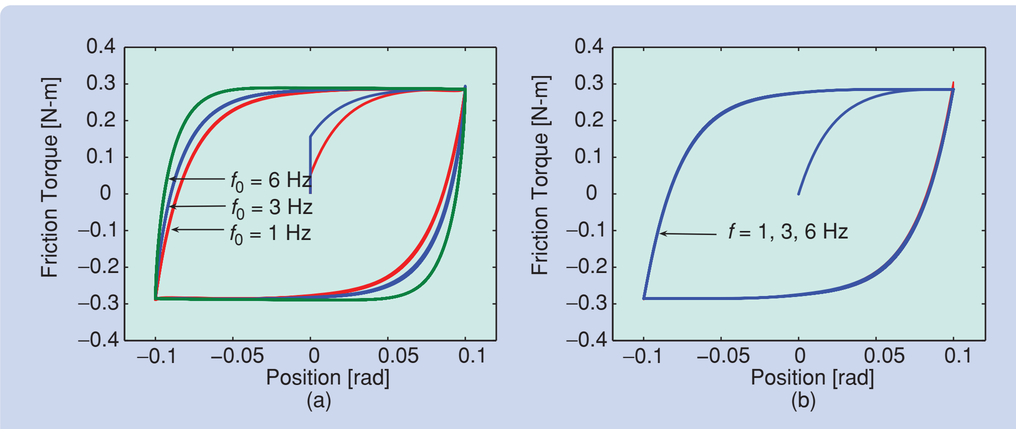

FIGURE 10 Behavior of the (a) LuGre and (b) Dahl models for sinusoidal inputs with frequencies of 1, 3, and 6 Hz. The plots show the friction force as a function of displacement. Notice that the curves generated by the Dahl model are rate independent, whereas the curves produced by the LuGre model depend on frequency. The difference is mainly due to the presence of the Stribeck component through the function $g(v)$ in the LuGre model.

Finally, we explore the effect of the spring stiffness k. It follows from (23) that changes in k shift the equilibrium horizontally, that is, moves to the left with increasing values of k. Figure 8 shows stick-slip behavior for several values of k. For small values of k the equilibrium (23)–(25) is asymptotically stable. The limit cycle is also asymptotically stable but large perturbations from the equilibrium are required to reach the limit cycle. The limit cycle disappears when the stiffness is sufficiently large but the equilibrium (23)–(25) remains asymptotically stable.

RATE INDEPENDENCE

The friction operator $H: v \mapsto F$ is *rate independent* if it is invariant with respect to affine transformation of the time scale. That is, H is rate independent if the input-output pair $(v(t), F(t))$ is an admissible solution of a rate-independent friction operator, then $(v(a+bt), F(a+bt))$ is also an admissible pair for all real a and positive b. An operator that does not satisfy such a property is *rate dependent*.

Simulations of the rate-independent Dahl model with periodic inputs in Figure 9(c)–(f) show that closed-curves in the $F-x$ plane are formed when the input is periodic with a dc component. These loops do not change when the frequency of the input is changed. They are shifted when a bias is added to the input signal but the shape does not change.

More generally, consider a friction model of the form

$$\frac{dF}{dt} = \chi(F, v) = \psi(F, \mathrm{sgn}(v))\eta(v), \qquad (28)$$

where $\eta(v)$ is positively homogeneous, that is, $\eta(\alpha v) = \alpha\eta(v)$ for all $\alpha > 0$. Changing the time scale by the transformation $\tau = \varphi(t)$, with the properties described in "Rate Independence of the Dahl Model," yields

$$\varphi'\left[\frac{dF}{d\tau} - \psi(F, \mathrm{sgn}(v))\eta(v_\tau)\right] = \varphi'\left[\frac{dF}{d\tau} - \chi(F, v_\tau)\right] = 0, \qquad (29)$$

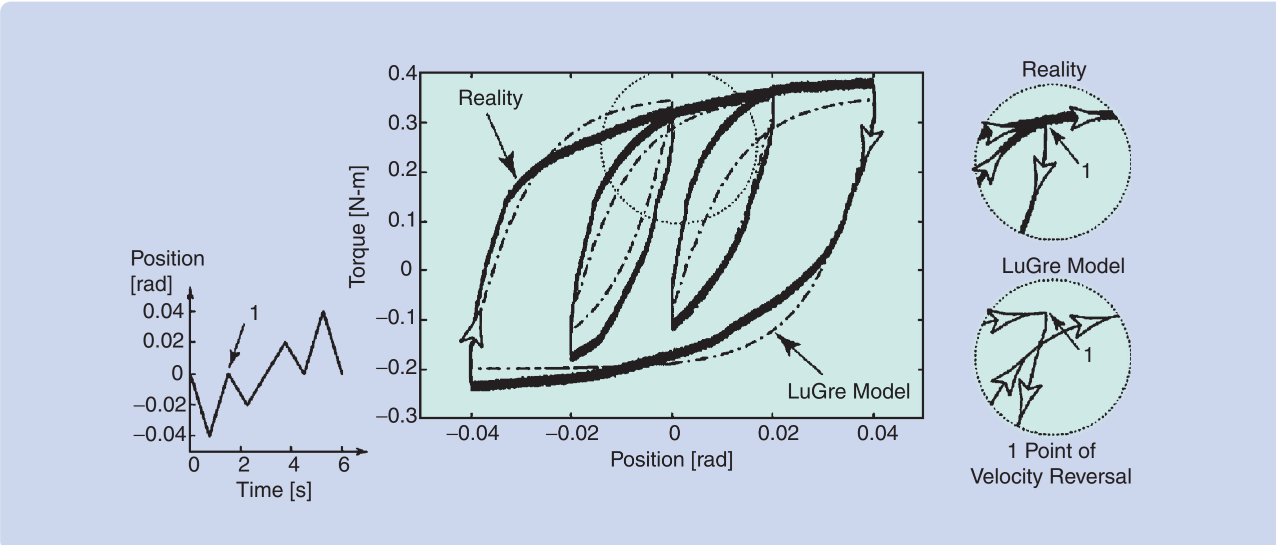

FIGURE 11 Experiments reported in [31] showing limitations of the LuGre model in predicting behavior at velocity reversals. The solid curve shows experimental data from a vertical electrodischarge machining axis. (Figure reproduced from [31] with permission from Dr. Altpeter.)

with $v_\tau \triangleq (dx/d\tau)$, and $\varphi' > 0$. It follows from (29) that solutions $(F(t), v(t))$ are invariant with respect to a positively homogeneous time scaling, and the model is thus rate independent.

The LuGre Model Is Rate Dependent

The LuGre model is rate dependent since the right-hand side of (1) is not affine in $|v|$; see [45]. This rate dependence is caused by the function $g(v)$, which captures the Stribeck effect. Figure 10 compares the rate dependencies of the Dahl and LuGre models. As expected, the loops in the $F - x$ plane obtained from the LuGre model are not invariant to changes in the velocity of the input. The differences between the shapes of these loops decrease as F_s approaches F_c. The presence of viscous friction σ_2 does not influence this behavior.

Figure 11 shows an experiment reported in [31], where experimental data from a vertical electrodischarge machining axis are compared to simulations using the LuGre model. The gross features of the experiment are captured by the LuGre model, but, as discussed above, the LuGre model is not rate independent and hence does not capture the reversal point memory observed experimentally.

CONCLUSIONS

In this article we have described some properties of the LuGre model, which is a dynamic friction model with a few parameters that can be fit by measuring steady-state friction as a function of velocity. The model has interesting theoretical properties, namely, the state is in a finite range, it has passivity properties, and is rate dependent. The LuGre model captures many properties of real friction behavior, but it does not have reversal point memory. The model has been used extensively for simulation and for designing friction compensators. In the article it is also shown that limit-cycle behavior in stick-slip motion are well described by the model. Rate dependence is also discussed. The analysis of rate-dependent microdamping, as well as rate dependency, are areas where the model can be improved.

REFERENCES

[1] F.P. Bowden and D. Tabor, *Friction—An Introduction to Tribology*. New York: Anchor Press/Doubleday, 1973.

[2] J. Israelachvili, *Intermolecular and Surface Forces*. New York: Academic, 1995.

[3] E. Rabinowicz, *Friction and Wear of Materials*. New York: Wiley, 1995.

[4] J.H. Dieterich, "Time-dependent friction in rocks," *J. Geophysical Res.*, vol. 77, pp. 3690–3697, 1972.

[5] F.P. Bowden and D. Tabor, *The Friction and Lubrication of Solids*. London, UK: Oxford Univ. Press, 1950.

[6] E. Rabinowicz, "The nature of the static and kinetic coefficients of friction," *J. Appl. Phys.*, vol. 22, no. 11, pp. 1373–79, 1951.

[7] R. Stribeck, "Die wesentlichen Eigenschaften der Gleit- und Rollenlager—The key qualities of sliding and roller bearings," *Zeitschrift des Vereins Deutscher Ingenieure*, vol. 46, no. 38–39, pp. 1342–1348, 1432–1437, 1902.

[8] J.R. Rice and A.L. Ruina, "Stability of steady frictional slipping," *J. Appl. Mech. Trans. ASME*, vol. 50, no. 2, pp. 343–349, 1983.

[9] J.-C. Gu, J.R. Rice, A.L. Ruina, and S.T. Tse, "Slip motion and stability of a single degree of freedom elastic system with rate and state dependent friction," *J. Mech. Phys. Solids*, vol. 32, no. 3, pp. 167–196, 1984.

[10] A.L. Ruina, "Slip instability and state variable friction laws," *J. Geophysical Res.*, vol. 88, no. B12, pp. 10359–10370, 1983.

[11] J. Krim, "Friction at the atomic scale," *Scientific Amer.*, vol. 275, no. 4, pp. 74–80, 1996.

[12] M. Mate, *Tribology on the Small Scale*. New York: Oxford Univ. Press, 2008.

[13] A. Tustin, "The effects of backlash and of speed-dependent friction on the stability of closed-cycle control systems," *J. Institution Electrical Engineers Part 1 General*, vol. 94, pp. 143–151, 1947.

[14] N.A. Osborne and D.L. Rittenhouse, "The modeling of friction and its effects on fine pointing control," in *Proc. AIAA Guidance, Navigation and Control Conf.*, Anaheim, CA, 1974, pp. 3928–3939.

[15] G. Brandenburg and U. Schäfer, "Influence and compensation of Coulomb friction in industrial pointing and tracking systems," in *Proc. 1991 IEEE Industry Applications Society Annu. Meeting.*, 1991, pp. 1407–1413.

[16] H. Olsson and K.J. Åström, "Friction generated limit cycles," *IEEE Trans. Contr. Syst. Technol.*, vol. 9, no. 4, pp. 629–636, 2001.

[17] C. Canudas de Wit, K.J. Åström, and K. Braun, "Adaptive friction compensation in DC motor drives," *IEEE J. Robot. Automat.*, vol. RA-3, no. 6, pp. 681–685, 1987.

[18] C. Canudas de Wit, "Robust control for servo-mechanisms under inexact friction compensation," *Automatica*, vol. 29, no. 3, pp. 757–761, 1993.

[19] B. Friedland and Y.-J. Park, "On adaptive friction compensation," in *Proc. IEEE Conf. Decision and Control*, 1991, pp. 2899–2902.

[20] H. Olsson, K.J. Åström, C. Canudas de Wit, M. Gäfvert, and P. Lischinsky, "Friction models and friction compensation," *Euro. J. Contr.*, vol. 3, pp. 176–195, 1998.

[21] B. Armstrong-Hélouvry, *Control of Machines with Friction*. Norwell, MA: Kluwer, 1991.

[22] P. Dupont, V. Hayward, B. Armstrong, and F. Altpeter, "Single state elasto-plastic friction models," *IEEE Trans. Automat. Contr.*, vol. 47, no. 5, pp. 787–792, 2002.

[23] P. Dahl, "A solid friction model," The Aerospace Corp., El Segundo, CA, Tech. Rep. TOR-0158(3107–18)-1, 1968.

[24] P.R. Dahl, "Solid friction damping of mechanical vibrations, " *AIAA J.*, vol. 14, pp. 1675–1682, 1996.

[25] P.R. Dahl and J.H. Ly, "Dynamic hysteresis modeling, " in *Proc. AIAA Modeling and Simulation Technologies Conf.*, Denver, CO, Aug. 2000, AIAA Paper AIAA-2000-4094, pp. 14–17.

[26] Z.P. Bazant and P. Bhat, "Endochonic theory of inelasticity and failure of concrete," *J. Eng. Meachanical Division ASCE*, vol. 12, no. EM4, pp. 701–722, 1976.

[27] C. Canudas de Wit, H. Olsson, K.J. Åström, and P. Lischinsky, "Dynamic friction models and control design, " in *Proc. 1993 American Control Conf.*, San Francisco, CA, 1993, pp. 1920–1926.

[28] C. Canudas de Wit, H. Olsson, K.J. Åström, and P. Lischinsky, "A new model for control of systems with friction," *IEEE Trans. Automat Contr.*, vol. 40, no. 3, pp. 419–425, Mar. 1995.

[29] H. Olsson, "Control systems with friction," Ph.D. dissertation, Dept. Automatic Control, Lund Institute of Technology, Lund, Sweden, 1996 [Online]. Available: http://www.control.lth.se/publications/

[30] R. Barabanov and N. Ortega, "Necessary and sufficient conditions for passivity of the LuGre friction model," *IEEE Trans. Automat. Contr.*, vol. 45, no. 4, pp. 830–832, 2000.

[31] F. Altpeter, "Friction modeling, identification and compensation," Ph.D. dissertation, Ecole Politechnique Federal de Lausanne, 1999 [Online]. Available: http://library.epfl.ch/ theses/?nr=1988

[32] C. Canudas de Wit and P. Lischinsky, "Adaptive friction compensation with partially known dynamic friction model," *Int. J. Adaptive Contr. Signal Process.*, vol. 11, no. 1, pp. 65–80, 1997.

[33] A. Shiriaev, A. Robertsson, and R. Johansson, "Friction compensation for passive systems based on the {LuGre} model," in *Proc. 2nd IFAC Workshop on Lagrangian and Hamiltonian Methods for Nonlinear Control*, Seville, Spain, Apr. 2003, pp. 183–188.

[34] P. Lischinsky, C. Canudas de Wit, and G. Morel, "Friction compensation for an industrial hydraulic robot," *IEEE Contr. Syst. Technol.*, vol. 19, no. 1, pp. 25–33, 1999.

[35] J. Swevers, F. Al-Bender, and E.-A. Ganseman, "An integrated friction model structure with improved presliding behavior for accurate friction compensation," *IEEE Trans. Automat. Contr.*, vol. 45, no. 4, pp. 675–686, 2000.

[36] F. Al-Bender, V. Lampaert, and J. Swevers, "The generalized Maxwell-slip model: A novel model for friction simulation and compensation," *IEEE Trans. Automat. Contr.*, vol. 50, no. 11, pp. 1883–1887, 2005.

[37] V. Lampaert, J. Swevers, and F. Al-Bender, "Modification of the Leuven integrated friction model structure," *IEEE Trans. Automat. Contr.*, vol. 47, no. 4, pp. 683–687, 2002.

[38] L.C. Bo and D. Pavelescu, "The friction–speed relation and its influence on the critical velocity of the stick-slip motion," *Wear*, vol. 82, no. 3, pp. 277–89, 1982.

[39] A. van der Schaft, *L_2-Gain and Passivity Techniques in Nonlinear Control.* Berlin, Germany: Springer-Verlag, 1999.

The LuGre model captures many properties of real friction behavior, but it does not have reversal point memory.

[40] C. Canudas de Wit and R. Kelly, "Passivity analysis of a motion control for robot manipulators with dynamic friction," *Asian J. Contr.*, vol. 9, no. 1, pp. 30–36, 2007.

[41] B. Armstrong-Hélouvry and X. Chen, "The Z-properties chart," *IEEE Contr. Syst. Mag.*, vol. 28, no. 5, pp. 79–89, 2008.

[42] P.-A. Bliman and M. Sorine, "A system-theoretic approach of systems with hysteresis. Application to friction modelling and compensation," in *Proc. 2nd European Control Conf.*, Groningen, The Netherlands, 1993, pp. 1844–49.

[43] P.-A. Bliman, "Mathematical study of the Dahl's friction model," *Euro. J. Mech. A/Solids*, vol. 11, no. 6, pp. 835–848, 1992.

[44] P.-A. Bliman and M. Sorine, "Easy-to-use realistic dry friction models for automatic control," in *Proc. 3rd European Control Conf.*, Rome, Italy, 1995, pp. 3788–3794.

[45] J.-H. Oh and D.S. Bernstein, "Semilinear Duhem model for rate-independent and rate-dependent hysteresis," *IEEE Trans. Automat. Contr.* vol. 50, no. 5, pp. 631–645, 2005.

[46] D.A. Haessig and B. Friedland, "On the modelling and simulation of friction," *J. Dyn. Syst. Meas. Contr. Trans. ASME*, vol. 113, no. 3, pp. 354–362, 1991.

AUTHOR INFORMATION

Karl Johan Åström (kja@control.lth.se) was educated at the Royal Institute of Technology, Stockholm, Sweden. After graduating he worked for five years for IBM Research. In 1965 he became a professor at Lund Institute of Technology/Lund University, where he founded the Department of Automatic Control. He has coauthored eight books and numerous articles covering a wide area of theory and applications. He is listed in ISAHighlyCited, and he is a fellow of IFAC and a Life Fellow of IEEE. He received the 1987 IFAC Quazza medal, the 1990 IEEE Control Systems Award, and the 1993 IEEE Medal of Honor. He can be contacted at the Department of Automatic Control, Lund University, Box 118, SE 221 00 Lund, Sweden.

Carlos Canudas-de-Wit (carlos.canudas-de-wit@gipsa-lab.inpg.fr) received the B.Sc. degree in electronics and communications from the Technological Institute of Monterrey, Mexico in 1980. In 1987 he received the Ph.D. in automatic control from the Department of Automatic Control, Institute Polytechnic of Grenoble, France. Since then he has been the director of research at the National Center for Scientific Research (CNRS), where he teaches and conducts research in the area of nonlinear control of mechanical systems and networked control system. His research interests include networked control systems, vehicle control, adaptive control, identification, control of robots, and systems with friction. He is a past associate editor of *IEEE Transactions on Automatic Control* and *Automatica*.